Accurate simulation of transient landscape evolution by eliminating numerical diffusion: the TTLEM 1.0 model

Benjamin Campforts[1], Wolfgang Schwanghart[2] and Gerard Govers[1]

[1] KU Leuven, Division Geography, Department of Earth and Environmental Sciences

[2] Universität Potsdam, Institute for Earth and Environmental Science

Correspondence to: benjamin.campforts@kuleuven.be

Abstract. Landscape evolution models (LEM) allow studying how the earth surface responses to changing climatic and tectonic forcings. While much effort has been devoted to the development of LEMs that simulate a wide range of processes, the numerical accuracy of these models has received less attention. Most LEMs use first order accurate numerical methods that suffer from substantial numerical diffusion. Numerical diffusion particularly affects the solution of the advection equation and thus the simulation of retreating landforms such as cliffs and river knickpoints with potential consequences for the integrated response of the simulated landscape. Here we test a higher order flux limiting finite volume method that is total variation diminishing (TVD-FVM) to solve the partial differential equations of river incision and tectonic displacement. We show that the choice of the TVD-FVM to simulate river incision significantly influences the evolution of simulated landscapes and the spatial and temporal variability of catchment wide erosion rates. Furthermore, a 2D TVD-FVM accurately simulates the evolution of landscapes affected by lateral tectonic displacement, a process whose simulation was hitherto largely limited to LEMs with flexible spatial discretization. We implement the scheme in TTLEM, a spatially explicit, raster based LEM for the study of fluvially eroding landscapes in TopoToolbox 2.

1. Introduction

Landscape evolution models (LEMs) simulate how the earth surface evolves in response to different driving forces including tectonics, climatic variability and human activity. LEMs are integrative as they amalgamate empirical data and conceptual models into a set of mathematical equations that can be used to reconstruct or predict terrestrial landscape evolution and corresponding sediment fluxes (Glotzbach, 2015; Howard, 1994). Studies that address how climate variability and land use changes will affect landscapes on the long term increasingly rely on LEMs (Gasparini and Whipple, 2014).

Landscape evolution is not always smooth and gradual. Instead, sudden tectonic displacements along tectonic faults can create distinct landforms with sharp geometries (Whittaker et al., 2007). These topographic discontinuities not necessarily smooth out over time, but may persist over long time scales in transient landscapes (Mudd, 2016; Vanacker et al., 2015). For example, faults may spawn knickpoints along river profiles. These knickpoints will propagate upstream as rapids or water falls (Hoke et al., 2007), thereby maintaining their geometry through time (Campforts and Govers, 2015). After an uplift pulse, the river will only regain a steady state when knickpoints finally arrive in the uppermost river reaches. Transiency is not limited to individual rivers but also affects entire orogens such as the Southern Alps of New Zealand where the landscape may never reach a condition of steady state due to the permanent asymmetry in vertical uplift, climatically driven denudation and horizontal tectonic advection (Herman and Braun, 2006).

Transient 'shocks' and topographic discontinuities are inherently difficult to model accurately. Most of the widely applied LEMs use first order accurate explicit or implicit finite difference methods to solve the partial differential equations (PDE) that are used to simulate river incision (Valters, 2016). These schemes suffer from numerical diffusion (Campforts and Govers, 2015; Royden and Perron, 2013). Numerical diffusion will inevitably lead to the gradual disappearance of knickpoints and will result in ever-smoother shapes. It has already been shown that numerical smearing decreases the

accuracy of modelled longitudinal river profiles (Campforts and Govers, 2015). Here, we hypothesize that it is also relevant for the simulation of hillslope processes: hillslopes respond to river incision and, thus, inaccuracies in river incision modelling will propagate to the hillslope domain. Whether and to what extent this occurs, is yet unexplored.

Tectonic displacement is similar to river knickpoint propagation; in both cases, sharp landscape forms are laterally moving. Numerical diffusion may therefore significantly alter landscape features when tectonic shortening or extension is simulated using first order accurate methods. In principle, flexible gridding overcomes this problem through dynamically adapting the density of nodes on the modelling domain to the local rate of topographic change. However, models using flexible gridding have other constraints. They are more difficult to implement and impose the structure of the numerical grid to the natural drainage network as rivers must follow the grid structure. Furthermore, the output of flexible grid models is not directly compatible with most software that is available for topographic analysis.

Here we present TTLEM, a spatially explicit raster based LEM, which is based on the object-oriented function library TopoToolbox 2 (Schwanghart and Scherler, 2014). Contrary to previously published LEMs we solve the stream power river incision model using a flux limiting finite volume method (FVM) which is total variation diminishing (TVD) in order to avoid numerical diffusion. Our numerical scheme expands on previous work (Campforts and Govers, 2015) by extending the mathematical formulation of the TVD method from 1D to entire river networks. Moreover, we develop a 2D TVD-FVM scheme to simulate horizontal tectonic displacement on regular grids, that enables simulation of three dimensional variations in tectonic deformation. The objective of this paper is to evaluate TTLEM and assess the performance of the numerical methods for a variety of real and simulated topographic and tectonic situations.

2. LEM components and geomorphic transport laws

2.1. Tectonic deformation

In its simplest form, tectonic processes are represented by their kinematics and the assumed vertical surface deformation field $U(x,y,t)$ [L t^{-1}]. However, many tectonic configurations imply that displacements have both a vertical (uplift or subsidence) and a lateral (extension or shortening) component (Willett, 1999; Willett et al., 2001). The change in elevation of the earth surface over time due to lateral tectonic displacement excluding vertical rock uplift $(\partial z/\partial t)_{td}$ is then:

$$\left(\frac{\partial z}{\partial t}\right)_{td} = \mathbf{u}\frac{\partial z}{\partial x} + \mathbf{v}\frac{\partial z}{\partial y} \tag{1}$$

where $\mathbf{u}$ and $\mathbf{v}$ [L T^{-1}] are the tectonic displacement velocities in the cardinal directions (horizontal $\mathbf{u}$ and vertical $\mathbf{v}$).

2.2. River incision

Detachment limited fluvial erosion $(\partial z/\partial t)_{fluv}$ is calculated with the stream power law (SPL) (Howard and Kerby, 1983):

$$\left(\frac{\partial z}{\partial t}\right)_{fluv} = -KA^m\left(\frac{\partial z}{\partial x_\Gamma}\right)^n \tag{2}$$

The equation is solved on a dendritic stream network domain Γ where x_Γ refers to the distance from the outlet. A [L^2] is catchment area and proxy for the local discharge, and K [L^{1-2m} t^{-1}] is an erodibility parameter that depends on local climate, hydraulic roughness, lithology and sediment load. m and n are the area and slope exponents: their values reflect hydrological conditions, channel width, as well as the dominant erosion mechanism. K, m and n are interdependent and it is usually impractical to constrain any of their values alone (Croissant and Braun, 2014; Lague, 2014). Thus, many studies provide

estimates for the m/n ratio. For m/n ratios between 0.35 and 0.8, K values span several orders of magnitude between 10^{-10} - 10^{-3} m$^{(1-2m)}$ yr^{-1} (Kirby and Whipple, 2001; Seidl and Dietrich, 1992; Stock and Montgomery, 1999).

2.3. Hillslope processes

River incision drives the development of erosional landscapes by setting the base level for hillslope processes. Steepening of hillslope toes leads to increased sediment fluxes from hillslopes to the river system. Hillslope denudation $(\partial z/\partial t)_{hill}$ is equal to the divergence of the flux of soil/regolith material ($\mathbf{q_s}$, [L^3 L^{-1} T^{-1}]):

$$\left(\frac{\partial z}{\partial t}\right)_{hill} = -\nabla \mathbf{q_s} \qquad (3)$$

Different geomorphological laws describe hillslope response to lowering base levels. The model of linear diffusion assumes that the soil/regolith flux is proportional to hillslope gradient ∇z (Culling, 1963):

$$\mathbf{q_s} = -D\nabla z \qquad (4)$$

where D is the diffusivity [L^2 t^{-1}] that parameterizes hillslope erodibility and determines rate of soil/regolith creep. Main controls on variations of D include substrate, lithology, soil depth, climate and biological activity. Values of D range between 10^{-3} and 10^{-1} m^2 yr^{-1} for slopes under natural land use (Campforts et al., 2016; DiBiase and Whipple, 2011; Jungers et al., 2009; Roering et al., 1999; West et al., 2013). Linear hillslope diffusion produces convex upward slopes. Field evidence, however, suggests that the linear diffusion model is only rarely appropriate (Dietrich et al., 2013). Instead, hillslopes often tend to have convex-planar profiles because rapid, ballistic particle transport and shallow landsliding dominate when slopes approach or exceed a critical angle (DiBiase et al., 2010; Larsen and Montgomery, 2012). To account for this rapid increase of flux rates with increasing slopes, Andrews and Bucknam (1987) and Roering et al. (1999) proposed a nonlinear formulation of diffusive hillslope transport, assuming that flux rates increase to infinity if slope values approach a critical slope S_c:

$$\mathbf{q_s} = -\frac{D\nabla z}{1-\left(\left|\nabla z\right|/S_c\right)^2} \qquad (5)$$

2.4. Final model

In summary, TTLEM solves the following PDE, whereby an explicit distinction is made between the fluvial and hillslope domain. The fluvial domain is determined by cells having a contributing drainage area exceeding a critical drainage area (A_c):

$$\frac{\partial z}{\partial t} = \left(\frac{\partial z}{\partial t}\right)_{td} + \begin{cases} U + \left(\dfrac{\partial z}{\partial t}\right)_{fluv} & \text{for } A \geq A_c \\ \dfrac{\rho_r}{\rho_s}U + \left(\dfrac{\partial z}{\partial t}\right)_{hill} & \text{for } A < A_c \end{cases} \qquad (6)$$

The detachment limited incision model assumes that rivers incise directly into bedrock and instantaneously excavate all material entering rivers from adjacent hillslopes. Material fluxes on slopes mobilize either soil or regolith that have different

bulk density than the bedrock. This is accounted for by multiplying the rock uplift rate with the density ratio between ρ_r and ρ_s [M L^{-3}] representing the bulk densities of the bedrock and the regolith material respectively (Perron, 2011).

3. Implementation and numerical schemes of TTLEM

We solve Eq. 6 using a set of numerical schemes that we implement in the software TopoToolbox Landscape Evolution Model (TTLEM) (see also Fig. A1). TTLEM is written in the MATLAB programming language and in C-code where this significantly improves performance (e.g. for the non-linear hillslope diffusion algorithm of Perron (2011)). Integrating TTLEM into TopoToolbox (Schwanghart and Kuhn, 2010; Schwanghart and Scherler, 2014) provides access to efficient algorithms of digital elevation models (DEMs) analysis, as well as numerous routines for visualizing and analyzing modelling outputs. In the following sections, we will discuss the numerical schemes of TTLEM to solve the PDEs described in previous section. The section numbers correspond to the processes indicated in the model flowchart in the appendix (Fig. A1).

3.1. Drainage network development

TopoToolbox provides a function library for deriving the drainage network and terrain attributes (Schwanghart and Scherler, 2014). The calculation of flow-related terrain attributes, i.e., data derived from flow directions, relies on a set of highly efficient algorithms that exploit the directed and acyclic graph structure of the river flow network (Phillips et al., 2015). Nodes of the network are grid cells and edges represent the directed flow connections between the cells in downstream direction. Topological sorting of this network returns an ordered list of cells in that upstream cells appear before their downstream neighbors. Based on this list, we calculate terrain attributes such as upslope area with a linear scaling thus enabling efficient calculation ($O(n)$) at each time step even for large grids (Braun and Willett, 2013).

DEMs of real landscapes frequently contain data artifacts that generate topographic sinks. Topographic sinks can also occur during simulations when diffusion on hillslopes creates "colluvial wedges" that dam sections of the river network. By adopting algorithms of flow network derivation from TopoToolbox, TTLEM makes use of an efficient and accurate technique for drainage enforcement to derive non-divergent (D8) flow networks (Schwanghart et al., 2013; Soille et al., 2003). Based on the thus derived flow network, TTLEM uses downstream minima imposition (Soille et al., 2003) that ensures that downstream pixels in the network have lower or equal elevations than their upstream neighbors.

3.2. Tectonic displacement

We implement a 2D version of a flux limiting total volume method to reduce numerical diffusion when simulating tectonic displacements on a regular grid. Equation (1) can be written as a scalar conservation law:

$$z_t + f(z)_u + f(z)_v = 0 \tag{7}$$

where $f(z)_u = \mathbf{u}z$ and $f(z)_v = \mathbf{v}z$ are the flux functions of the conserved variable z. We refer to the supplementary material of Campforts and Govers (2015) for a derivation of the differential form of Eq. (7) which can be converted to a numerical semi-conservative flux scheme:

$$z_{i,j}^{k+1} = z_{i,j}^{k} + \frac{\Delta t}{\Delta x}\left[f_{i-\frac{1}{2},j} - f_{i+\frac{1}{2},j} \right] + \frac{\Delta t}{\Delta y}\left[f_{i,j-\frac{1}{2}} - f_{i,j+\frac{1}{2}} \right] \tag{8}$$

where $z_{i,j}^k$ is the elevation of the cell at row i and column j at time $k \times \Delta t$. f represents the numerical approximation of the physical fluxes from Eq. (7). The in- and out coming fluxes are approximated with a flux limiting upwind method which is

135   TVD. A TVD scheme prevents the total variation of the solution to increase in time and hence prevents spurious oscillations that are associated with higher order numerical methods (Toro, 2009). The flux limiter entails that the method has a hybrid order of accuracy being second order accurate in most cases but shifting to first order accuracy near discontinuities. Hence the TVD-FVM method achieves two desirable properties: a higher order of accuracy than first order schemes and high numerical stability (Harten, 1983). TTLEM uses a staggered Cartesian grid for numerical discretization. The DEM grid

140   centers represent the center of the computational cells, whereas the velocity fields ($\mathbf{u}$ and $\mathbf{v}$) are located at the cell faces.

The numerical TVD fluxes are calculated following Toro (2009). In the following, we illustrate how to derive the flux over one cell boundary:

$$f_{i+\frac{1}{2},j}^{TVD} = f_{i+\frac{1}{2},j}^{LO} + \varphi_{i+\frac{1}{2},j}\left[f_{i-\frac{1}{2},j}^{HI} - f_{i+\frac{1}{2},j}^{LO} \right] \tag{9}$$

where f^{HI} and f^{LO} represent the high and low order fluxes respectively:

$$f_{i+\frac{1}{2},j}^{LO} = \alpha_0 v_{i+\frac{1}{2},j} z_{i,j}^k + \alpha_1 v_{i+\frac{1}{2},j} z_{i+1,j}^k$$

$$f_{i+\frac{1}{2},j}^{HI} = \beta_0 v_{i+\frac{1}{2},j} z_{i,j}^k + \beta_1 v_{i+\frac{1}{2},j} z_{i+1,j}^k \tag{10}$$

The low order fluxes are solved with a first order explicit upwind Godunov scheme (1959):

$$\alpha_0 = \frac{1}{2}\left(1 + sign\left(\mathbf{v}\right)\right) \quad\text{and}\quad \alpha_1 = \frac{1}{2}\left(1 - sign\left(\mathbf{v}\right)\right) \tag{11}$$

145   The high order fluxes are solved with a Lax-Wendroff scheme (1960):

$$\beta_0 = \frac{1}{2}\left(1 + \mathbf{v}\frac{\Delta t}{\Delta x}\right) \quad\text{and}\quad \beta_1 = \frac{1}{2}\left(1 - \mathbf{v}\frac{\Delta t}{\Delta x}\right) \tag{12}$$

From Eq. (10), Eq. (11) and Eq. (12) it follows that:

$$f_{i+\frac{1}{2}}^{LO} = v_{i+\frac{1}{2},j} z_{i+1}^k$$

$$f_{i+\frac{1}{2}}^{HI} = \frac{1}{2} v_{i+\frac{1}{2},j}\left(z_i^k + z_{i+1}^k\right) - \frac{\left(v_{i+\frac{1}{2},j}\right)^2 \Delta t}{2\Delta x}\left(z_{i+1}^k - z_i^k\right) \tag{13}$$

$\varphi_{i+\frac{1}{2},j}$ represents the flux limiter, which is solved with the van Leer scheme (1997):

$$\varphi_{i+\frac{1}{2},j} = \frac{r_{i+\frac{1}{2},j} + abs\left(r_{i+\frac{1}{2},j}\right)}{1 + abs\left(r_{i+\frac{1}{2},j}\right)}$$

(14)

where r is a smoothness index calculated as:

$$r_{i+\frac{1}{2},j} = \frac{z_{i+2,j}^{k} - z_{i+1,j}^{k}}{z_{i+1,j}^{k} - z_{i,j}^{k}}$$

(15)

The overall performance of the TVD-FVM is evaluated by comparing it with the first order accurate upwind Godunov scheme (Godunov, 1959), which is not flux limiting Eq. (11). In the remaining part of the text, we refer to this scheme as the first order Godunov Method (GM).

3.3. River incision

3.3.1. Numerical solution

TTLEM features a 1D version of the flux limiting TVD-FVM to solve for river incision (Eq. (2)) which is written as a scalar conservation law:

$$z_t + f(z)_x = 0$$

(16)

where $f(z)$ represents the flux function of the conserved variable z, representing the river elevation. The method resembles the one described in the previous section but differs in that fluxes are calculated in one direction on a directed acyclic graph (Phillips et al., 2015). We refer to the Supplementary Information provided by Campforts and Govers (2015) for a full derivation of this scheme.

In addition, we implement a first order implicit FDM for the solution of the SPL detailed in Braun and Willett (2013). The method provides stable solutions regardless of the time step length, a property desired when simulating landscape evolution over long timescales and large spatial domains. Explicit schemes of river incision (both FDM and TVD-FDM), in turn, require time steps that satisfy the Courant Friedrich Lewy condition (CFL):

$$\frac{u_{max}\Delta t}{\Delta x} \leq 1$$

(17)

where u_{max} is the maximum velocity dictated by few river cells with high drainage areas. Compared to these velocities, hillslope processes modelled by the linear diffusion equation are usually slow. Applying longer time steps for hillslope processes is a computational advantage that an implicit scheme increases even more (Pelletier 2008). TTLEM thus uses two time steps: an outer time step (Δt_{outer}) during which hillslope processes and the planform river network are calculated, and an inner time step (Δt_{inner}) nested within the outer time step that used to solve for river incision. Thus, while Δt_{outer} should satisfy the CFL criterion for the explicit linear or nonlinear diffusion equation, the Δt_{inner} is flexible and adheres to the CFL criterion of the explicit river incision equation (Supplement Fig. 1). The adoption of implicit methods allows relaxing both time step constraints. Yet, TTLEM allows setting limits to Δt_{outer} and Δt_{inner}, and enables us to investigate the impact of the length of the time step on model outcomes (see section 5.1.2).

3.3.2. Analytical solution

Ideally, numerical methods are benchmarked against analytical solutions. Albeit available for specific initial and boundary conditions only, analytical solutions are accurate and grid resolution independent, contrary to numerical solutions where model parameter values might depend on the grid resolution (Pelletier, 2010). We implemented an analytical solution for the SPL as an independent benchmark to compare the performance of the different numerical schemes of river incision under conditions where an analytical solution is available.

First, we created an artificial DEM with topography in steady state between uplift and erosion (see Table 1). From this DEM, we extracted the drainage network and corresponding river elevations by selecting all cells exceeding 10^6 m^2. Very short river profiles (<10 km) are excluded from the analysis. Subsequently, we simulate landscape evolution using the numerical models documented in the previous sections assuming spatially invariant uplift rates. After each simulation, we obtain river elevations from the resulting DEMs and compare them with river elevations that we derived analytically using the pre-uplift, steady state river profiles as input. Analytical solutions for the stream power law are based on the slope patch method of Royden and Perron (2013) that non-dimensionalizes the stream power law using a dimensionless height (λ) and transformed horizontal distance metric χ:

$$\lambda = \frac{z_x}{h_0} \tag{18}$$

$$\chi = \frac{A_0^{m/n}}{h_0} \int_0^x \frac{dx}{A_x^{m/n}} \tag{19}$$

where z_x represents the dimensionless elevation along the river profile, h_0 is a reference length scale (set to 1 m) and A_0 is a reference value for the drainage area (set to 1×10^6 m²). To integrate over abrupt changes in the drainage area along the rivers, Eq. (19) is solved using the rectangle rule (Mudd et al., 2014). Steady state river profiles appear as straight lines in this non-dimensional coordinate system. The analytical slope patch solution then calculates the evolution of a dimensionless river profile in response to uplift. The method is detailed in the appendix of Royden and Perron (2013) and based on tracing individual patches which are initiated at the outlet of the drainage network and propagate upstream with a velocity dictated by upstream area and the parameters of the SPL (Eq.(2)).

We calculated the slope patch solution to the steady-state pre-uplift river profiles using the simulated uplift rates as input, and assessed the accuracy of the numerical methods with the Root Mean Squared Error (RMSE):

$$RMSE = \sqrt{\frac{\sum_{i=1}^{n}\left(z_{i,analytical} - z_{i,numerical}\right)^2}{n_{riv}}} \tag{20}$$

where $z_{i,analytical}$ and $z_{i,numerical}$ refer to the analytically and numerically calculated elevation of a river cell respectively and n_{riv} is the total number of river cells.

3.4. Hillslope processes

We implemented linear hillslope diffusion using the implicit Crank-Nicolson scheme (Pelletier, 2008). The scheme is unconditionally stable at large time steps A numerical solution of the nonlinear hillslope equation, however, is more demanding. The maximum time step length of an explicit FDM sharply decreases as slopes approach the threshold gradient. To overcome this restriction, Perron (2011) developed Q-imp, an implicit solver that allows to increase the time step lengths by several orders of magnitude. Whereas the per-operation computational cost of this algorithm is higher in comparison to

the explicit solution, the overall performance of this method is better than alternative solutions (Perron, 2011). Q-imp efficiently calculates hillslope diffusion even for high-resolution simulations. However, rapid incision during one time step may generate slopes along rivers that are greater than the threshold slope, a situation that Q-imp cannot solve. An approach is thus needed that adjusts hillslopes to the threshold slope prior to calculating Q-imp.

210 We assume that hillslopes instantaneously adjust to oversteepening by mobilising the amount of material required to reduce the slope gradient to the threshold value S_c (Burbank et al., 1996). We refrain from simulating individual landslides although we acknowledge that single high magnitude low frequency events may be relevant at the time scales of our simulations (Korup, 2006). Instead, our approach implicitly accounts for the combined effects of a large number and variety of landslides that effectively adjust slopes to a threshold slope. This threshold slope can be thought of "an average effective angle of

215 internal friction which controls hillslope stability" (Burbank et al., 1996). We implement this hillslope adjustment using a modified version of the excess topography algorithm (Blöthe et al., 2015). In this algorithm, elevations z at time step $t + 1$ are calculated so that the absolute local gradient at each grid cell becomes less or equal than S_c. This is achieved by decreasing elevations at location i to the minimum elevation of all other locations j to which we add an offset calculated as the product of the Euclidean distance $\|i,j\|$ and S_c:

$$z_i^{t+1} = \min\left\{z_i^t, \min\left[z_j^t + S_c \cdot \|i, j\|\right]\right\} \qquad (21)$$

220 The above equation entails that z_i^{t+1} at one location depends on all other grid cells and that the algorithm has a time complexity of $O(N^2)$, which would render it unsuitable for frequent updating during LEM simulations. To avoid an excessively high computational load, we implement the algorithm using morphological erosion with a gray-scale structuring element (see MATLAB function ordfilt2), which is a minimum sliding window with additive offsets calculated from the window size and Sc. This significantly reduces run times as we calculate elevations at one location from the sliding window.

225 Yet, this approach may retain gradients greater than S_c at steep and long slope sections. We solve this by calling the algorithm repeatedly until all slope values are equal or less than S_c.

4. Impact of numerical methods

We investigate how numerical schemes implemented in TTLEM affect simulated landscape evolution. As we focus on

230 evaluating the schemes' performance, all simulations have synthetically generated landscapes as initial surfaces. Hence, our simulations are uncalibrated and results remain untested against an actual landscape: however, the chosen parameter values are within the range of previous studies (e.g. Gasparini and Whipple, 2014; Whipple and Tucker, 1999). We distinguish between the effects on simulated river incision on the one hand and on simulated tectonic displacement on the other. To investigate the accuracy and implications of river incision methods, we compare the explicit TVD-FVM with the first-order

235 implicit FDM and further differentiate between the implicit FDM where no limitation is set on the time step and the implicit FDM where the CFL criterion limits the time step length. To investigate the accuracy and implications of river incision methods we compare an explicit first order Godunov method (GM) with the 2D TVD-FVM.

4.1. River incision

4.1.1. 1D river incision

240 The impact of numerical diffusion on propagating river profile knickpoints is most obvious in situations where an analytical solution is available. The first simulation illustrates such a situation, with an artificial river profile characterized by a major knickzone between 8 and 12 km from the river head (Fig. 1). We assume that the drainage area is increasing in proportion to

the square of the distance and uplift equals zero. For this simplified configuration, an analytical solution for the SPL relies on the method of characteristics (Luke, 1972). Notwithstanding the relatively high spatial resolution of 100 m, the first order implicit FDM suffers from considerable numerical diffusion when river incision is calculated over a time span of 1 Myr (Fig. 1). The TVD-FVM systematically achieves a much higher accuracy over a wide range of spatial resolutions and parameter values (Campforts and Govers, 2015).

4.1.2. Drainage network

We assess the numerical accuracy of the entire drainage network with spatially and temporally constant values for all model parameter values (Table 1) and assuming a fixed drainage network (see section 3.3.2). We first create a steady-state artificial landscape (Fig. 2) on a 50 km × 100 km grid with a spatial resolution of 100 m that we initialize with uniformly distributed random elevation values between 0 and 50 m (Movie S1). Our simulation uses Dirichlet boundary conditions and inserts a spatially and temporally uniform vertical uplift of 1 km Myr^{-1} over a period of 150 Myr. Δt_{outer} is set to 5×10^4 yr.

Following steady state, we impose four consecutive sinusoidal uplift pulses of equal magnitude to this artificial landscape over 1 Myr. Each uplift pulse has a wavelength of 0.25 Myr and an amplitude of 3×10^{-3} m yr^{-1} (Fig. 3). We repeat the simulations with three different numerical schemes (implicit FDM without time step limitation, implicit FDM with time step limitation (CFL condition applied) and TVD-FVM), each at 22 different spatial resolutions (6.25, 12.5, 25, 50, 100, 150, …, 950 m). Hillslopes are simulated using linear hillslope diffusion in combination with threshold slopes, a configuration typically used to simulate landscape evolution at geological timescales (e.g. Goren et al., 2014). The threshold slope is set to 0.8 m m^{-1} and hillslope diffusivity is 0.01 m^{2}y^{-1}. We record the CPU time required to run a 1 Myr simulation to assess computational performance. In order to facilitate the high resolution run (at 6.25 m where the spatial domain covers 7950 × 15950 cells) all model runs were executed on one computational node of the Flemish Super Cluster (VSC) using a single core (Broadwell, E5-2680v4) and 128 Gb RAM. We evaluate the numerical performance of the schemes and the impact of spatial resolution against an analytical solution (slope patch method) for the entire drainage network represented by all cells exceeding 1 km^2 (Fig. 2).

Figure 4 compares results obtained from the numerical methods and the analytical solution. The initial river profiles slightly differ depending on spatial resolution due to interpolation of the steady-state artificial landscape with a spatial resolution of 100 m. The results show that TVD-FVM and implicit numerical solutions converge at increasing spatial resolutions. Where the time step of the implicit scheme is unbounded by the CFL criterion, however, the solution deviates from those adhering to the CFL criterion. This illustrates that there is trade-off between numerical accuracy and numerical stability for an implicit scheme at long time steps. In addition, an implicit scheme at high spatial resolution and large time steps fails to converge to an analytical solution because uplift is modelled as a discrete stepwise rather than a continuous function (e.g. the sinusoidal uplift history used here) that inserts artificial shocks in the solution.

The TVD-FVM is consistently more accurate than the implicit methods at all spatial resolutions although the implicit FDM (CFL<1) approaches the high accuracy of the TVD-FVM at very high resolutions (6.25 m) (Fig. 5a). At lower spatial resolutions (>10 m) the numerical accuracy of the TVD-FVM is significantly higher compared to the accuracy obtained with the implicit methods at the cost of a slightly increased additional computation time. To achieve the same numerical accuracy as the TVD-FVM at 500 m spatial resolution (RMSE = 18.17, model runtime = 2.89 seconds), the implicit method (CFL<1) would need to be evaluated at 150 m which would take 12 times longer (model runtime = 36 sec) (Fig. 5b).

4.1.3. River incision and catchment-wide erosion rates

We hypothesize that the diffusive nature of commonly applied first order FDM is not restricted to the simulation of river longitudinal profiles but has systematic consequences for other measures derived from LEM simulations. Such measures

include catchment-wide erosion rates that constitute the basis for model-field data comparison and model parametrization (Gasparini and Whipple, 2014; Moon et al., 2015). In order to investigate the sensitivity of LEM-derived catchment-wide erosion rates to different numerical schemes of the river incision model, we use the steady-state artificial landscape described in the previous experiments (section 4.1.2). The simulation runs over 5 Myr with four consecutive uplift pulses of equal amplitude and a wavelength of 1.25 Myr with Dirichlet boundary conditions and a planform fixed drainage network. We use two spatial resolutions (100 m and 500 m) and three different numerical methods (implicit FDM without time step limitation, implicit FDM with time step limitation (CFL condition applied) and TVD-FVM) to simulate river incision. The maximum length of Δt_{inner} is set to 3×10^3 yr for all schemes to ensure that the implicit method is converging at higher resolutions, too (see section 4.1.2). Hillslope response is simulated using a linear diffusion scheme in combination with a threshold slope (S_c, see Fig. A2).

We compare differences in simulated erosion rates by randomly selecting >200 catchments with drainage areas ranging between 1 and 50 km^2 (Fig. 7). We calculate the erosion rates for each time step by subtracting the elevation grid in the previous time step from the updated, current, elevation grid. The sum of elevation differences within each catchment refers to the catchment-wide erosion rate integrated over the time step length. For each catchment, we then derive the difference between erosion rates calculated by the different numerical schemes and summarize them using the RMSE statistics ($O_{TVD\text{-}FDM}$):

$$O_{TVD-FDM} = \sqrt{\frac{\sum_{i=1}^{n} \left(\varepsilon_{i,TVD} - \varepsilon_{i,FDM} \right)^2}{nb_{\Delta t}}} \tag{22}$$

where $\varepsilon_{i,TVD}$ and $\varepsilon_{i,FDM}$ refer to the catchment wide erosion rates simulated with the TVD-FVM and FDM respectively to simulate river incision and $nb_{\Delta t}$ is the total number of discrete time steps of the simulated erosion record.

We rank the catchments in increasing order of $O_{TVD\text{-}FDM}$ for each simulation to investigate variations in catchment wide erosion rates. Fig. 6 shows the results for the catchments at 10%, 50% (median) and 90% percentile. Ranks are derived separately for the models runs at 100 m and 500 m as different catchments are randomly generated for both simulation runs. The percentiles shown in Fig. 6 therefore represent different catchments.

For most catchments, we detect differences in catchment-wide erosion rates between the three numerical methods at a spatial resolution of 100 m. Generally, the amplitude of the response to a tectonic uplift pulse increases when using TVD-FVM: the use of a first order implicit FDM without time step restriction results in a much smoother response in comparison to the TVD-FVM. The variations in response amplitude are significant: the majority of the catchments record amplitude reductions by more 50% when modelled with the implicit FDM without time step restriction. Time step restriction (and thereby sacrificing the main advantage of the implicit FDM) significantly reduces numerical diffusion so that most catchments display an erosional response comparable to that simulated by the TVD-FVM. However, this is only true for simulations with a 100 m spatial resolution. The advantage of a time step restricted implicit FDM over a non-restricted implicit FDM disappears almost completely for a coarser grid resolution of 500 m.

Figure 7 shows that erosion rates diverge between the different methods with increasing distance to the outlet of the main river while they are similar for larger catchments. A smaller effect of the numerical scheme on large catchment areas may partly arise from stronger averaging of local variations in catchment erosion rates. In addition, catchments at a large distance from the outlet—and thus likely with smaller catchment areas—will experience upstream migrating knickpoints only after several model time steps. If catchments are far from the fault zone, knickpoints will then be significantly smoothed by a first order accurate implicit FDM, which will ultimately affect the response of the catchment. Again, spatial resolution matters: a

larger grid size not only results in larger differences on average but also in larger differences between small and large catchments (Fig. 7).

The differences in catchment response relate to the differences in simulated erosion rates within the catchments. Figure 8 illustrates the spatial difference in erosion rates calculated with the two numerical methods during the final step of the model run (after 5 Myr). This figure shows that spatial differences are significant and form a systematic banded pattern related to the upslope migration of the erosion waves of the individual uplift pulses.

4.2. Tectonic displacement

We test the performance of the 2D version of the flux limiting TVD-FVM to simulate tectonic displacement. A synthetic DEM forms the initial surface for a simulation of a constant lateral tectonic displacement with neither fluvial incision nor hillslope diffusion. Theoretically, this should result in a laterally displaced landscape that, apart from this displacement, remains unchanged in comparison to the initial state. We compare the flux limiting TVD-FVM with a first order accurate upwind Godunov Method (GM) simulating a tectonic displacement in two directions ($\mathbf{u} = \mathbf{v} = 10$ mm yr^{-1}) over a time span of 1 Myr. Fig. 9 illustrates that the explicit GM strongly smooths the resulting DEM whereas the 2D TVD-FVM scheme produces a DEM that is very similar to the initial DEM, with reduced amounts of numerical diffusion.

In order to quantify the amount of numerical diffusion (D_N [L^2 yr^{-1}]) introduced by the GM and the TVD-FVM method, we test a range of different model configurations and calculate the numerical diffusivity, D_N, corresponding to the observed smoothing. D_N is the diffusivity required to transform the initial DEM (DEM_{ini}) to the final DEMs produced at the end of the simulations (DEM_{fint}). The optimum amount of diffusion is determined by minimizing the misfit function H with a sequential quadratic programming method (Nocedal and Wright, 1999). H is given by:

$$H = \sqrt{\frac{\sum_{px=1}^{nb_{px}}\left(DEM_{ini} - DEM_{f\,int}\right)^2}{nb_{px}}} \qquad (23)$$

where nb_{px} is the number of pixels in the DEM.

We find that numerical diffusivity of the GM exceeds commonly used values of hillslope diffusivities as soon as spatial resolution exceeds 90 m (Fig. 10a). The 2D TVD-FVM decreases numerical diffusion by a factor of 5-60 compared to the GM (Fig. 10b). The accuracy increases for both schemes with increasing resolution and increasing CFL numbers. Yet, the gain in accuracy with increasing spatial resolution is higher for the TVD-FVM than for the GM. Our analysis shows that the explicit FDM performs best with a CFL criterion close to one where additional required iterations within a given time interval are at a minimum (Gulliver, 2007).

5. Discussion

Our analysis of numerical solvers focusses on three interrelated issues: numerical accuracy, spatial resolution and computational efficiency. Adopting highly simplifying assumptions allow us to benchmark the solvers against analytical solutions. Our focus is on testing an implicit, first order accurate, FDM against TVD-FVM. The implicit FDM has several desirable properties. It is unconditionally stable and tolerates time step lengths exceeding those prescribed by the CFL criterion. LEMs are often run over time spans of millions of years and the CFL criterion is dictated by a few grid cells with high upslope areas. Adopting an implicit scheme is therefore potentially interesting as it allows decreasing the computation time while enabling simulations at high spatial resolutions. Our results, however, show that this major advantage vanishes if the aim of a LEM simulation is to capture transiency correctly. For CFL > 1, the implicit FDM introduces significant

numerical smearing, and for CFL >> 1, the approach tends to insert artificial shockwaves of uplift because gradual uplift is approximated by a step function if time steps are (very) large.

360 For time step lengths approaching those prescribed by the CFL criterion, we show that computational gains by implicit FDM are marginal compared to TVD-FVM. The TVD-FVM code can be vectorized, i.e. it exploits single-instruction multiple-data parallelism to save CPU time. The implicit FDM requires a lower number of numerical operations but all stream network nodes need to be treated sequentially. Simulations at higher spatial resolutions increase the numerical accuracy and may balance the low accuracy of the implicit, first order accurate, FDM. Our results indicate that there is indeed a strong gain in
365 numerical accuracy for all methods (Fig. 4 and 5) with increasing spatial resolution. However, to achieve the same numerical accuracy as the TVD-FVM, the implicit method with a CFL<1 constraint requires the use of spatial resolution that is about three times higher, resulting in a computation time that is ~12 times higher (Fig. 5). In summary, while a first order implicit scheme is stable and accurate for long-term, steady-state solutions (Braun and Willett 2013), it has severe shortcomings when simulating transient landscape evolution caused by knickpoint propagation in detachment limited erosional basins.
370 These shortcomings can, to a large extent, be avoided by using a TVD-FVM.

We also show that the impact of the numerical scheme used to simulate river incision is not limited to river profile development alone. Hillslopes adjust to local base level changes dictated by river incision. Hillslope denudation rates therefore must—at least partly— reflect the geometry and dynamics of a knickpoint and will respond differently to a diffuse
375 signal that is the result of relatively slow, continuous uplift on the one hand and a sharp discontinuity caused by a rapid base level drop of major fault activity on the other hand. Our simulations show that, depending on the spatial and temporal resolution, catchment wide erosion rates are more responsive to uplift when fluvial incision is calculated by TVD-FVM rather than by the, first order accurate, implicit FDM. This is because first order (explicit and implicit) FDMs fail to properly reproduce transient incision waves (Campforts and Govers, 2015) due to knickpoint smoothing. This also affects hillslope
380 denudation as the drop in hillslope base level due to the passage of a knickpoint is smeared out in time when smoothing occurs. The response of catchment wide erosion rates to uplift will therefore also be smoothed, resulting in significantly lower peak erosion rates. This effect will be most significant in upstream catchments which are far away from the base level as smoothing increases with time and knickpoint migration distance.

385 One might question the significance and necessity of numerical schemes that avoid diffusion of retreating knickpoints. Given the many assumptions and uncertainties that underlie many LEMs, numerical accuracy may seem a problem of lesser importance. We argue that the simulations presented in this paper show that this is not the case and that it is indeed critical to simulate knickpoint retreat as accurately as possible. However, our analysis does not cover all situations wherein the accurate simulation of knickzones is important. Simulation of sharp knickpoints is also required in geomorphological and
390 lithological settings where knickpoint retreat is caused by rock toppling, possibly triggered during extreme flood events (Baynes et al., 2015; Lamb et al., 2014; Mackey et al., 2014). Similarly, glacial incision often creates hanging valleys which are reshaped by migrating fluvial knickpoints after glacial retreat (Valla et al., 2010). In all these cases simulation tools with a minimum of numerical diffusion are required to correctly quantify natural knickpoint diffusion and to study the underlying processes.

395 First order numerical methods also inadequately simulate lateral tectonic displacement on a regular grid. The amount of numerical diffusion that is introduced by these methods will, in many cases, exceed natural diffusion rates, thus making accurate simulation of hillslope development impossible. A 2D variant of the TVD-FVM reduces the amount of numerical diffusion to values well below natural diffusivity values, an effect that is especially apparent at high spatial resolutions. The

2D TVD-FVM thus allows to accurately model this process, that significantly impacts the evolution of topography and river networks (Willett, 1999), using a fixed grid. This was hitherto only possible with flexible spatial discretization schemes.

Although most LEMs use first order accurate discretization schemes (Valters, 2016), the problem of numerical diffusion has been discussed in the broader geophysical community (Durran, 2010; Gerya, 2010). An alternative family of shock capturing Eulerian methods are MPDATA advection schemes (Jaruga et al., 2015). These schemes are based on a two-step approach in which the solution is first approximated with a first order upwind numerical scheme and then corrected by adding an antidiffusion term (Pelletier, 2008). However, contrary to the TVD-FVM, the standard MPDATA scheme (Smolarkiewicz, 1983) is not monotonicity preserving (i.e. it is not TVD). Instead, MPDATA introduces dispersive oscillations in the solution if combined with a source term (such as uplift) in the equation (Durran, 2010). Adding limiters to the solution of the antidiffusive step (Smolarkiewicz and Grabowski, 1990) renders the MPDATA scheme oscillation free (Jaruga et al., 2015). However, by adding this additional correction, the method approaches the numerical nature of the TVD-FVM which does not require further adjustments in any case.

Some of the weaknesses of the tested numerical solutions can be reduced by using LEMs that rely on irregular grid geometries. Irregular grids, for example, allow to simulate tectonic shortening using a Lagrangian approach where grid nodes are advected with the tectonically imposed velocity field (e.g. Herman and Braun, 2006). In TTLEM the TVD-FVM solvers are implemented using a fixed grid, which has several advantages. First, input data such as topography, climate, lithology or tectonic displacement fields are typically available as raster datasets and thus require only minor modifications whereas irregular grids require substantial preprocessing. Second, TTLEM output can instantly be analyzed and visualized using the TopoToolbox library (Schwanghart and Kuhn, 2010; Schwanghart and Scherler, 2014) or any other geographic information system. Thus, while irregular grid geometries and flexible grids may have some advantages over rectangular grids, TTLEM's implementation of numerically accurate algorithms strongly reduce the shortcomings of rectangular grids while facilitating straightforward processing of model in- and output.

6. Conclusion

Despite the growing interest in the development and use of LEMs, accuracy assessment of the numerical methods has received little attention. First order accurate FDM are the most commonly applied numerical methods. However, they introduce numerical diffusion and artificially smooth discontinuities that are inherent in transient landscapes. To overcome this problem, we developed the TVD-FVM. The TVD-FVM solves river incision more accurately than the first order accurate FDM's with significant influences on the geometry of modelled river profiles and implications for catchment wide erosion rates. Errors due to numerical diffusion depend on the spatial and temporal resolution as well as on the position of the catchment in the landscape. In addition, we introduce a 2D version of the TVD-FVM that allows simulating lateral tectonic displacement with low numerical diffusion on a fixed computational domain. Our new numerical techniques are implemented in the open access raster based Landscape Evolution Model (TTLEM) contained within TopoToolbox. Together with numerical implementations of common hillslope process models, TTLEM provides the community with a novel simulation tool for the accurate reconstruction, exploration and prediction of landscape evolution. In its current form, TTLEM is limited to uplifting, fluvially eroding landscapes. Further development will integrate other processes (e.g. glacial erosion) as well as the explicit routing of sediment through the landscape.

Code availability

TTLEM 1.0 is part of TopoToolbox version 2.2. The source code and future updates are available on the GIT repository https://github.com/wschwanghart/topotoolbox. TTLEM is platform independent and requires MATLAB 2014b or higher and the Image Processing Toolbox. Documentation and user manuals for the most current release version of TopoToolbox and TTLEM can be found at the GIT repository in the help folders of the software. The user manual of TTLEM includes three tutorials which can be accessed from the command window in MATLAB. The source code for the solution of the one dimensional Stream Power Law (SPLM) can be downloaded from the GIT repository https://github.com/BCampforts/SPLM. SPLM contains the solution of the 1D river incision codes including four examples.

Acknowledgements

This work was motivated by the meeting "Landscape evolution modelling - bridging the gap between field evidence and numerical models" in Hannover, 21-23, October 2015, that was organized by the *FACSIMILE* network and funded by the Volkswagen Foundation. Additional support comes from the Belgian Science Policy Office in the framework of the Interuniversity Attraction Pole project (P7/24): SOGLO - The soil system under global change. Numerical simulations were performed in the MATLAB environment (2015b) using numerical schemes as referred to in the text. Computational resources and services used to evaluate model performance were provided by the VSC (Flemish Supercomputer Center), managed by the Research Foundation - Flanders (FWO) in partnership with the five Flemish university associations. We are grateful to the IDYST group of the University of Lausanne and in particular Frédéric Herman and Aleksandar Licul for inspiring discussions on numerical methods and Nadja Stalder for the figure design. We further thank Taylor Perron for sharing his source code. We also thank two anonymous reviewers and the editor for constructive feedback that improved the manuscript.

Appendix

Model structure

The model architecture of TTLEM is illustrated in Fig. A1.

Hillslope processes

We illustrate the impact of different hillslope process models on simulated landscape evolution, using a 30 m resolution DEM of the Big Tujunga region in California as an example (Fig A2). TTLEM allows to simulate hillslope processes assuming (non)-linear slope dependent diffusion with the consideration of a threshold hillslope. Figure A2 illustrates how different hillslope process algorithms affect the evolution of hillslopes in the Big Tujunga region, California (Fig. A2a). We assume no tectonic displacement and use standard parameter values for river incision and hillslope diffusion (Table 1) and a threshold slope (S_c) of 1.2 (m/m) when applicable (Fig. A2b). We illustrate model results after 500 ky in Fig. 2c-d using the current topography as the starting condition. Linear diffusion (Eq. (4)) is not capable to keep up with river incision, which results in strongly oversteepened hillslopes near the river channels (Fig. A2c and 1g). While higher values for the diffusion coefficient D will eliminate this problem (e.g. Braun and Sambridge, 1997) they are incompatible with experimental findings (Roering et al., 1999) and will restrict hillslopes to convex upward shapes. The use of non-linear diffusion in combination with a threshold slope results in hillslopes similar to those simulated with linear diffusion in combination with a threshold slope. However, for a similar value of D, hilltops become more smoothed assuming non-linear diffusion as sediment fluxes due to diffusive processes now reach higher values when hillslopes approach the threshold slope.

The authors declare that they have no conflict of interest.

References

490   Andrews, D. J. and Bucknam, R. C.: Fitting degradation of shoreline scarps by a nonlinear diffusion model, J. Geophys. Res., 92(B12), 12857, doi:10.1029/JB092iB12p12857, 1987.

Baynes, E. R. C., Attal, M., Niedermann, S., Kirstein, L. a., Dugmore, A. J. and Naylor, M.: Erosion during extreme flood events dominates Holocene canyon evolution in northeast Iceland, Proc. Natl. Acad. Sci., 112(8), 201415443, doi:10.1073/pnas.1415443112, 2015.

495   Blöthe, J. H., Korup, O. and Schwanghart, W.: Large landslides lie low: Excess topography in the Himalaya-Karakoram ranges, Geology, 43(6), 523–526, doi:10.1130/G36527.1, 2015.

Braun, J. and Sambridge, M.: Modelling landscape evolution on geological time scales: A new method based on irregular spatial discretization, Basin Res., 9(1), 27–52, doi:10.1046-j.1365-2117.1997.00030.x, 1997.

Braun, J. and Willett, S. D.: A very efficient O(n), implicit and parallel method to solve the stream power equation governing
500   fluvial incision and landscape evolution, Geomorphology, 180–181, 170–179, doi:10.1016/j.geomorph.2012.10.008, 2013.

Burbank, D. W., Leland, J., Fielding, E., Anderson, R. S., Brozovic, N., Reid, M. R. and Duncan, C.: Bedrock incision, rock uplift and threshold hillslopes in the northwestern Himalayas, Nature, 379(6565), 505–510, doi:10.1038/379505a0, 1996.

Campforts, B. and Govers, G.: Keeping the edge: A numerical method that avoids knickpoint smearing when solving the stream power law, J. Geophys. Res. Earth Surf., 120(7), 1189–1205, doi:10.1002/2014JF003376, 2015.

505   Campforts, B., Vanacker, V., Vanderborght, J., Baken, S., Smolders, E. and Govers, G.: Simulating the mobility of meteoric 10Be in the landscape through a coupled soil-hillslope model (Be2D), Earth Planet. Sci. Lett., 439, 143–157, doi:10.1016/j.epsl.2016.01.017, 2016.

Croissant, T. and Braun, J.: Constraining the stream power law: a novel approach combining a landscape evolution model and an inversion method, Earth Surf. Dyn., 2(1), 155–166, doi:10.5194/esurf-2-155-2014, 2014.

510   Culling, W. E. H.: Soil Creep and the Development of Hillside Slopes, J. Geol., 71(2), 127–161, doi:10.1086/626891, 1963.

DiBiase, R. A. and Whipple, K. X.: The influence of erosion thresholds and runoff variability on the relationships among topography, climate, and erosion rate, J. Geophys. Res. Earth Surf., 116(F4), F04036, doi:10.1029/2011JF002095, 2011.

DiBiase, R. A., Whipple, K. X., Heimsath, A. M. and Ouimet, W. B.: Landscape form and millennial erosion rates in the San Gabriel Mountains, CA, Earth Planet. Sci. Lett., 289(1–2), 134–144, doi:10.1016/j.epsl.2009.10.036, 2010.

515   Dietrich, W. E., Bellugi, D. G., Sklar, L. S., Stock, J. D., Heimsath, A. M. and Roering, J. J.: Geomorphic Transport Laws for Predicting Landscape form and Dynamics, in Prediction in Geomorphology, edited by P. R. Wilcock and R. M. Iverson, pp. 103–132, American Geophysical Union: Washington, DC., 2013.

Durran, D. R.: Numerical Methods for Fluid Dynamics, Springer New York, New York, NY., 2010.

Gasparini, N. M. and Whipple, K. X.: Diagnosing climatic and tectonic controls on topography: Eastern flank of the northern
520   Bolivian Andes, Lithosphere, (May), 230–250, doi:10.1130/L322.1, 2014.

Gerya, T.: Introduction to Numerical Geodynamic Modelling, Cambridge University Press., 2010.

Glotzbach, C.: Deriving rock uplift histories from data-driven inversion of river profiles, Geology, 43(6), 467–470, doi:10.1130/G36702.1, 2015.

Godunov, S. K.: A Finite Difference Method for the Computation of Discontinuous Solutions of the Equations of Fluid
525   Dynamics, Math. USSR-Sbornik, 47(89), 271–306, 1959.

Goren, L., Willett, S. D., Herman, F. and Braun, J.: Coupled numerical-analytical approach to landscape evolution modeling, Earth Surf. Process. Landforms, 39(4), 522–545, doi:10.1002/esp.3514, 2014.

Gulliver, J. S.: Introduction to Chemical Transport in the Environment, Cambridge University Press, Cambridge., 2007.

Harten, A.: High resolution schemes for hyperbolic conservation laws, J. Comput. Phys., 49(3), 357–393, doi:10.1016/0021-
530   9991(83)90136-5, 1983.

Herman, F. and Braun, J.: Fluvial response to horizontal shortening and glaciations: A study in the Southern Alps of New

Zealand, J. Geophys. Res., 111(F1), F01008, doi:10.1029/2004JF000248, 2006.

Hoke, G. D., Isacks, B. L., Jordan, T. E., Blanco, N., Tomlinson, A. J. and Ramezani, J.: Geomorphic evidence for post-10 Ma uplift of the western flank of the central Andes 18°30′-22°S, Tectonics, 26(5), doi:10.1029/2006TC002082, 2007.

535   Howard, A. D.: A detachment-limited model of drainage basin evolution, Water Resour. Res., 30(7), 2261–2285, doi:10.1029/94WR00757, 1994.

Howard, A. D. and Kerby, G.: Channel changes in badlands, Geol. Soc. Am. Bull., 94(6), 739, doi:10.1130/0016-7606(1983)94<739:CCIB>2.0.CO;2, 1983.

Jaruga, A., Arabas, S., Jarecka, D., Pawlowska, H., Smolarkiewicz, P. K. and Waruszewski, M.: libmpdata++ 1.0: a library 540   of parallel MPDATA solvers for systems of generalised transport equations, Geosci. Model Dev., 8(4), 1005–1032, doi:10.5194/gmd-8-1005-2015, 2015.

Jungers, M. C., Bierman, P. R., Matmon, A., Nichols, K., Larsen, J. and Finkel, R.: Tracing hillslope sediment production and transport with in situ and meteoric 10 Be, J. Geophys. Res., 114(F4), 1–16, doi:10.1029/2008JF001086, 2009.

Kirby, E. and Whipple, K.: Quantifying differential rock-uplift rates via stream profile analysis, Geology, 29(5), 415, 545   doi:10.1130/0091-7613(2001)029<0415:QDRURV>2.0.CO;2, 2001.

Korup, O.: Rock-slope failure and the river long profile, Geology, 34(1), 45, doi:10.1130/G21959.1, 2006.

Lague, D.: The stream power river incision model: evidence, theory and beyond, Earth Surf. Process. Landforms, 39(1), 38–61, doi:10.1002/esp.3462, 2014.

Lamb, M. P., Mackey, B. H. and Farley, K. a: Amphitheater-headed canyons formed by megaflooding at Malad Gorge, 550   Idaho, Proc. Natl. Acad. Sci. U. S. A., 111(1), 57–62, doi:10.1073/pnas.1312251111, 2014.

Larsen, I. J. and Montgomery, D. R.: Landslide erosion coupled to tectonics and river incision, Nat. Geosci., 5(7), 468–473, doi:10.1038/ngeo1479, 2012.

Lax, P. and Wendroff, B.: Systems of conservation laws, Commun. Pure Appl. Math., 13(2), 217–237, doi:10.1002/cpa.3160130205, 1960.

555   van Leer, B.: Towards the Ultimate Conservative Difference Scheme, J. Comput. Phys., 135(2), 229–248, doi:10.1006/jcph.1997.5704, 1997.

Luke, J. C.: Mathematical models for landform evolution, J. Geophys. Res., 77(14), 2460–2464, doi:10.1029/JB077i014p02460, 1972.

Mackey, B. H., Scheingross, J. S., Lamb, M. P. and Farley, K. A.: Knickpoint formation, rapid propagation, and landscape 560   response following coastal cliff retreat at the last interglacial sea-level highstand: Kaua'i, Hawai'i, Geol. Soc. Am. Bull., 126(7–8), 925–942, doi:10.1130/B30930.1, 2014.

Moon, S., Shelef, E. and Hilley, G. E.: Recent topographic evolution and erosion of the deglaciated Washington Cascades inferred from a stochastic landscape evolution model, J. Geophys. Res. Earth Surf., 120(5), 856–876, doi:10.1002/2014JF003387, 2015.

565   Mudd, S. M.: Detection of transience in eroding landscapes, Earth Surf. Process. Landforms, n/a-n/a, doi:10.1002/esp.3923, 2016.

Mudd, S. M., Attal, M., Milodowski, D. T., Grieve, S. W. D. and Valters, D. a.: A statistical framework to quantify spatial variation in channel gradients using the integral method of channel profile analysis, J. Geophys. Res. Earth Surf., 119(2), 138–152, doi:10.1002/2013JF002981, 2014.

570   Nocedal, J. and Wright, S. J.: Numerical Optimization, Springer, New York., 1999.

Pelletier, J. D.: Quantitative Modeling of Earth Surface Processes, Cambridge University Press, Cambridge., 2008.

Pelletier, J. D.: Minimizing the grid-resolution dependence of flow-routing algorithms for geomorphic applications, Geomorphology, 122(1–2), 91–98, doi:10.1016/j.geomorph.2010.06.001, 2010.

Perron, J. T.: Numerical methods for nonlinear hillslope transport laws, J. Geophys. Res., 116(F2), F02021,

575   doi:10.1029/2010JF001801, 2011.

Phillips, J. D., Schwanghart, W. and Heckmann, T.: Graph theory in the geosciences, Earth-Science Rev., 143, 147–160, doi:10.1016/j.earscirev.2015.02.002, 2015.

Roering, J. J., Kirchner, J. W. and Dietrich, W. E.: Evidence for nonlinear, diffusive sediment transport on hillslopes and implications for landscape morphology, Water Resour. Res., 35(3), 853–870, doi:10.1029/1998WR900090, 1999.

580   Royden, L. and Perron, T. J.: Solutions of the stream power equation and application to the evolution of river longitudinal profiles, J. Geophys. Res. Earth Surf., 118(2), 497–518, doi:10.1002/jgrf.20031, 2013.

Schwanghart, W. and Kuhn, N. J.: TopoToolbox: A set of Matlab functions for topographic analysis, Environ. Model. Softw., 25(6), 770–781, doi:10.1016/j.envsoft.2009.12.002, 2010.

Schwanghart, W. and Scherler, D.: Short Communication: TopoToolbox 2 – MATLAB-based software for topographic

585   analysis and modeling in Earth surface sciences, Earth Surf. Dyn., 2(1), 1–7, doi:10.5194/esurf-2-1-2014, 2014.

Schwanghart, W., Groom, G., Kuhn, N. J. and Heckrath, G.: Flow network derivation from a high resolution DEM in a low relief, agrarian landscape, Earth Surf. Process. Landforms, 38(13), 1576–1586, doi:10.1002/esp.3452, 2013.

Seidl, M. and Dietrich, W.: The problem of channel erosion into bedrock, Catena, 23(Supplement), 101–124, 1992.

Smolarkiewicz, P. K.: A Simple Positive Definite Advection Scheme with Small Implicit Diffusion, Mon. Weather Rev.,

590   111(3), 479–486, doi:10.1175/1520-0493(1983)111<0479:ASPDAS>2.0.CO;2, 1983.

Smolarkiewicz, P. K. and Grabowski, W. W.: The multidimensional positive definite advection transport algorithm: nonoscillatory option, J. Comput. Phys., 86(2), 355–375, doi:10.1016/0021-9991(90)90105-A, 1990.

Soille, P., Vogt, J. and Colombo, R.: Carving and adaptive drainage enforcement of grid digital elevation models, Water Resour. Res., 39(12), doi:10.1029/2002WR001879, 2003.

595   Stock, J. D. and Montgomery, D. R.: Geologic constraints on bedrock river incision using the stream power law, J. Geophys. Res., 104(B3), 4983, doi:10.1029/98JB02139, 1999.

Toro, E. F.: Riemann solvers and numerical methods for fluid dynamics-A Practical Introduction, Springer, New York., 2009.

Valla, P. G., van der Beek, P. A. and Lague, D.: Fluvial incision into bedrock: Insights from morphometric analysis and

600   numerical modeling of gorges incising glacial hanging valleys (Western Alps, France), J. Geophys. Res. Earth Surf., 115(F2), F02010, doi:10.1029/2008JF001079, 2010.

Valters, D.: Modelling Geomorphic Systems: Landscape Evolution, in Geomorphological Techniques, vol. 12, edited by S. J. Cook, L. E. Clarke, and J. M. Nield, pp. 1–24, British Society for Geomorphology, London, UK., 2016.

Vanacker, V., von Blanckenburg, F., Govers, G., Molina, A., Campforts, B. and Kubik, P. W.: Transient river response,

605   captured by channel steepness and its concavity, Geomorphology, 228, 234–243, doi:10.1016/j.geomorph.2014.09.013, 2015.

West, N., Kirby, E., Bierman, P., Slingerland, R., Ma, L., Rood, D. and Brantley, S.: Regolith production and transport at the Susquehanna Shale Hills Critical Zone Observatory, Part 2: Insights from meteoric 10 Be, J. Geophys. Res. Earth Surf., 118(3), 1877–1896, doi:10.1002/jgrf.20121, 2013.

610   Whipple, K. X. and Tucker, G. E.: Dynamics of the stream-power river incision model: Implications for height limits of mountain ranges, landscape response timescales, and research needs, J. Geophys. Res. Solid Earth, 104(B8), 17661–17674, doi:10.1029/1999JB900120, 1999.

Whittaker, A. C., Cowie, P. A., Attal, M., Tucker, G. E. and Roberts, G. P.: Contrasting transient and steady-state rivers crossing active normal faults: New field observations from the central apennines, Italy, Basin Res., 19(4), 529–556,

615   doi:10.1111/j.1365-2117.2007.00337.x, 2007.

Willett, S. D.: Orogeny and orography: The effects of erosion on the structure of mountain belts, J. Geophys. Res. Solid Earth, 104(B12), 28957–28981, doi:10.1029/1999JB900248, 1999.

Willett, S. D., Slingerland, R. and Hovius, N.: Uplift , Shortening , and Steady State Topography in Active Mountain Belts, Am. J. Sci., 301(April/May), 455–485, doi:10.2475/ajs.301.4-5.455, 2001.

620
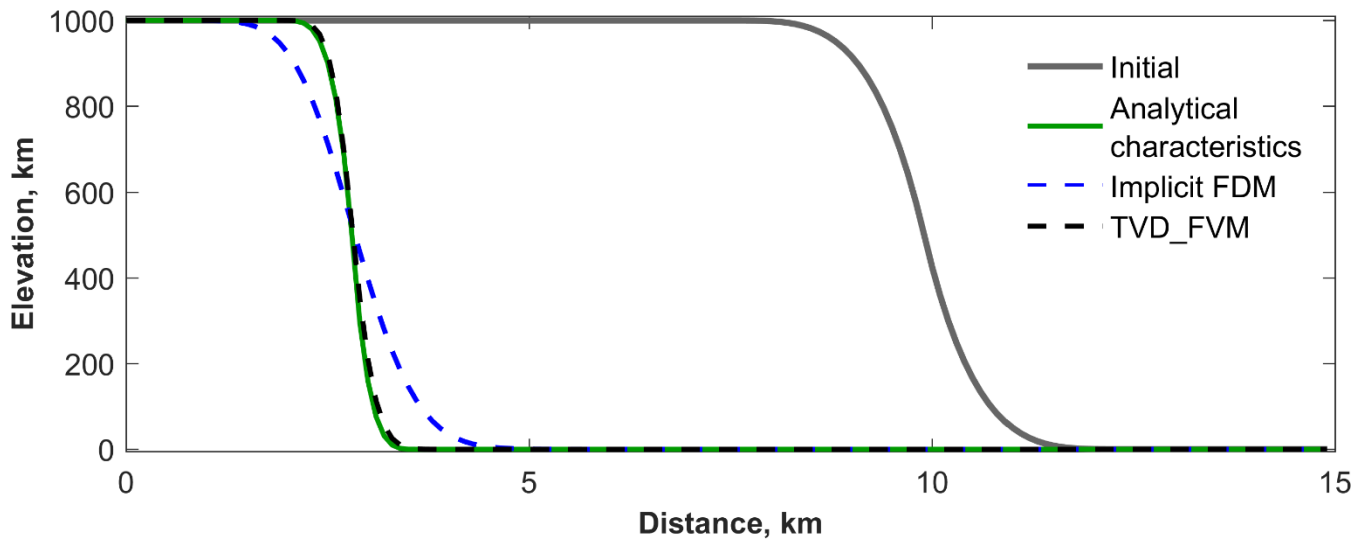
Figure 1. Solution of the linear 1D stream power law for a synthetic knickzone over a time span of 1 Myr. The analytical solution is obtained with the method of characteristics. The spatial resolution is 100 m. Table 1 lists other model parameter values.

625
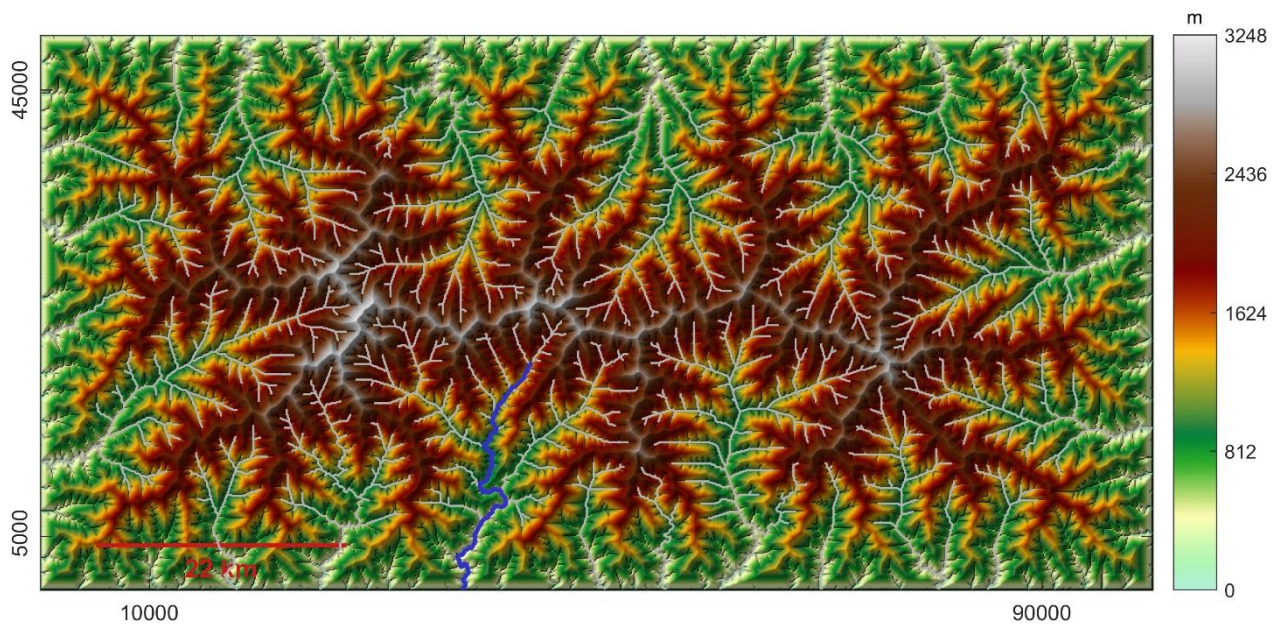
Figure 2. A synthetic steady state landscape produced as the testing environment to verify and compare the different numerical schemes implemented in TTLEM. Model runtime was 150 Myr, uplift rate was assumed to be spatially uniform over the area (block uplift) and fixed to 1 km Myr^{-1}. Other model parameter values are listed in Table 1. Dynamic landscape evolution is presented in Movie S1. The grey lines indicate the drainage network for which the solution has been calculated analytically as a benchmark solution. The blue line indicates the river profile for which model results at different resolutions are plotted in Fig. 4.

630
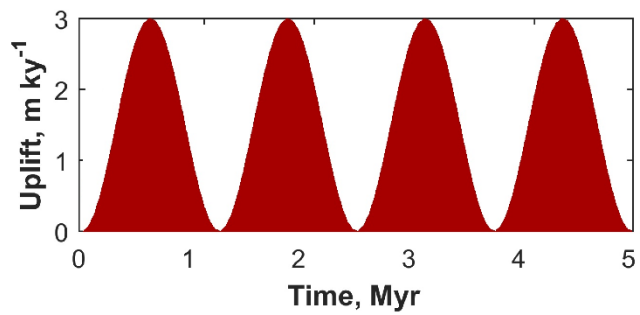
635 **Figure 3.** Uplift imposed to the steady state landscape shown in Figure 2 to investigate the impact of different numerical schemes.
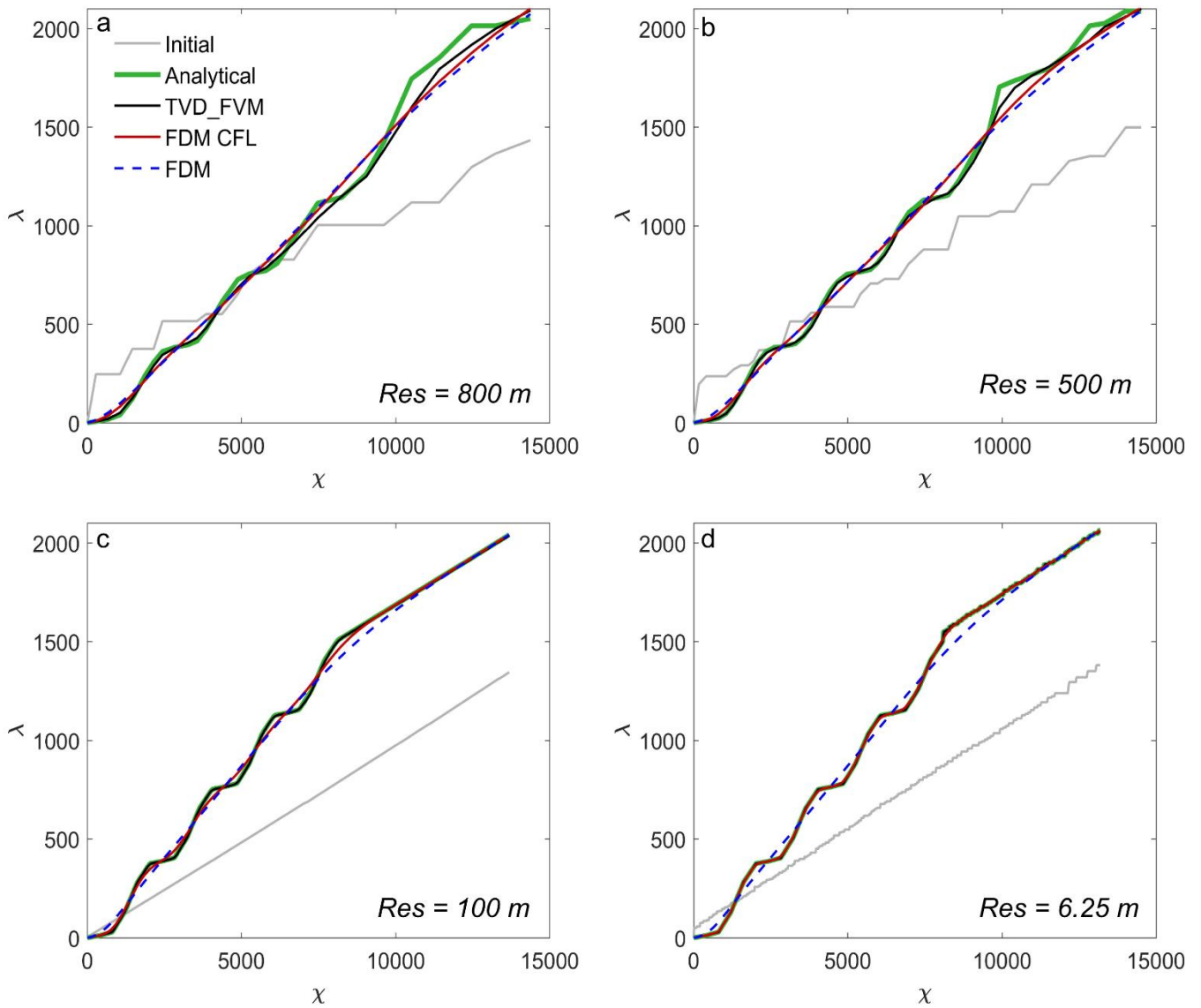
Figure 4: Comparison between different modelled resolutions for the river profile indicated in blue on figure 2. The green line is the analytical, 'true' solution, obtained with the slope patch method of Royden and Perron (2013). The full red line represents the first order accurate implicit solution when the CFL<1 and the dotted blue line represents the first order accurate implicit solution when the time step is left free. The implicit solutions where CFL<1 are simulated with a time step equal to the time step used for the TVD-FVM.
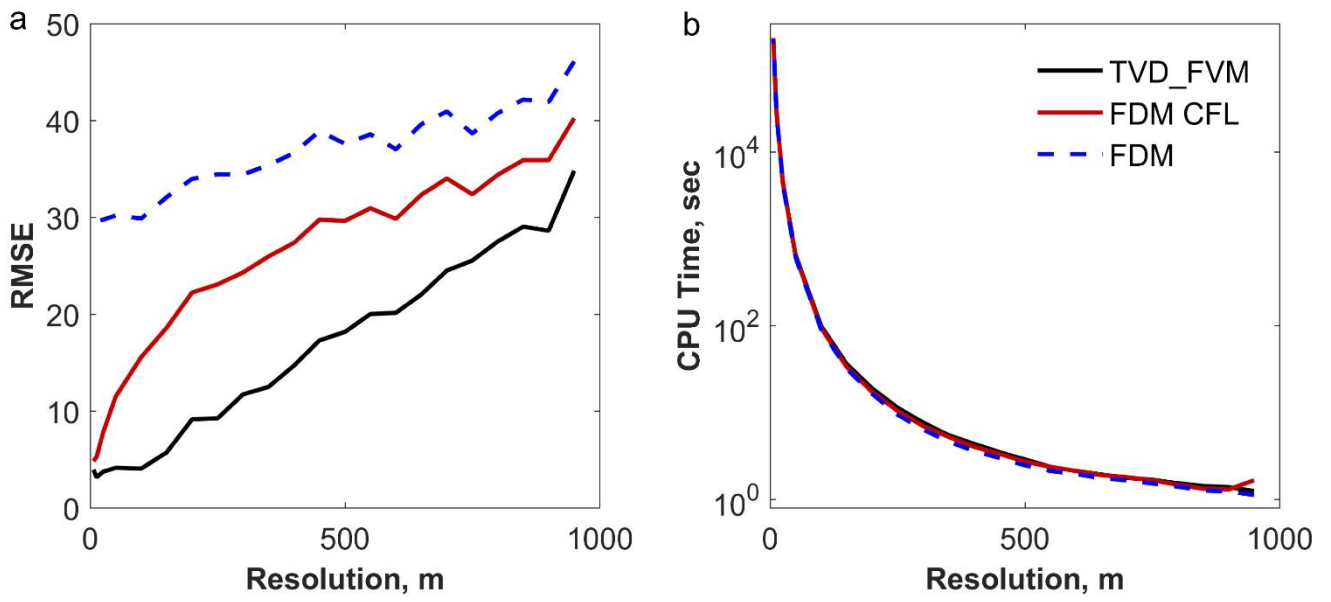
Figure 5: a. Performance of the different numerical schemes where the RMSE is calculated between the analytical and numerical methods. b. CPU time required to perform the model runs at the indicated resolutions.

650
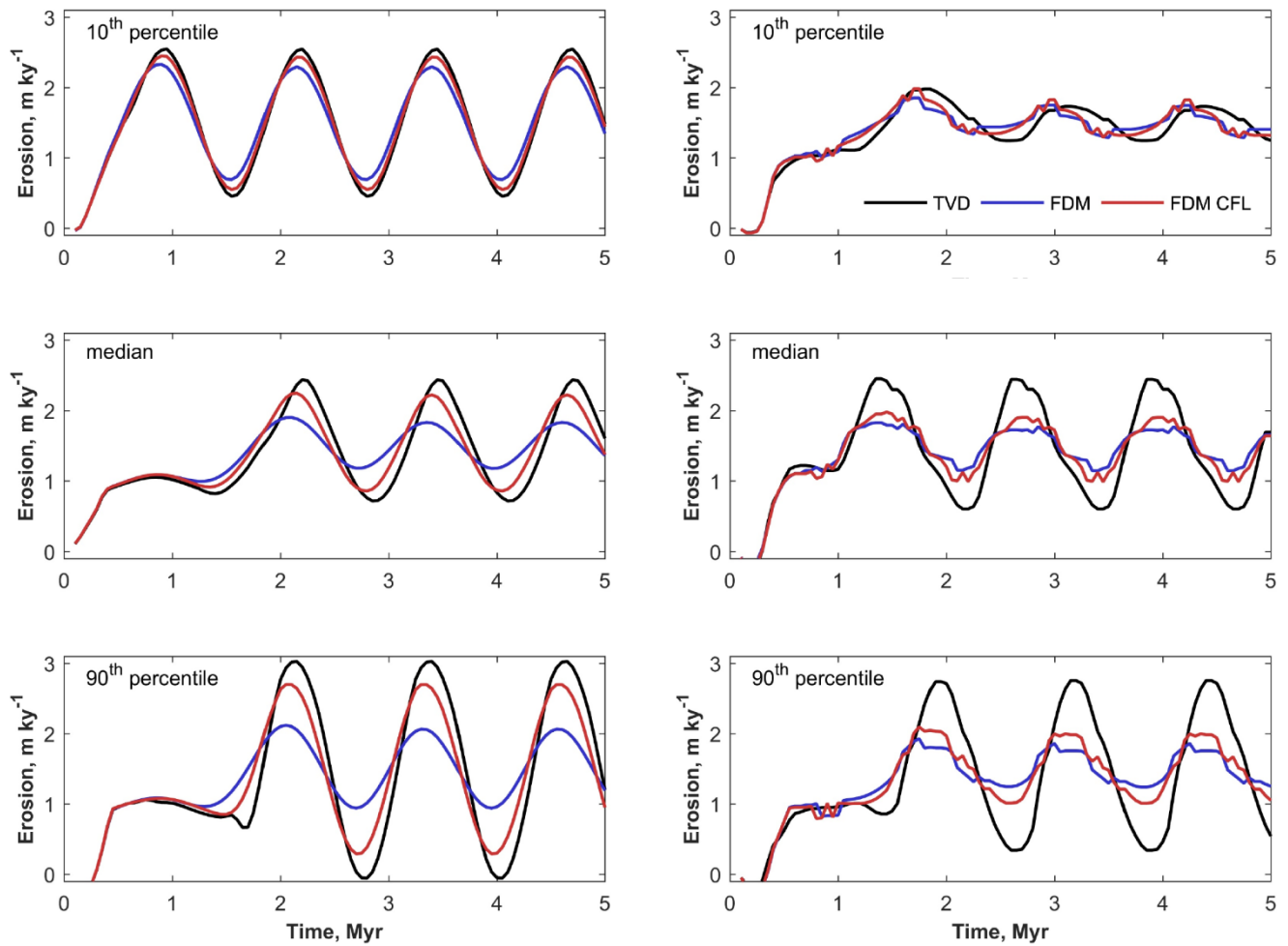
Figure 6. Temporal variation in simulated catchment wide erosion rates using different numerical methods to simulate river incision. The black lines represent simulations where a flux limiting TVD-FVM is used, the blue lines represent the first order accurate implicit FDM without constraints on the time steps and the red lines represent the first order accurate FDM with an inner time step calculated with the CFL criterion. (a) Simulations performed at a spatial resolution of 100 m. (b) Simulations performed at a spatial resolution of 500 m. Here, a median filter with a window of 3 time steps is applied to the simulated erosion rates to eliminate spikes which might occur at low resolutions.

655
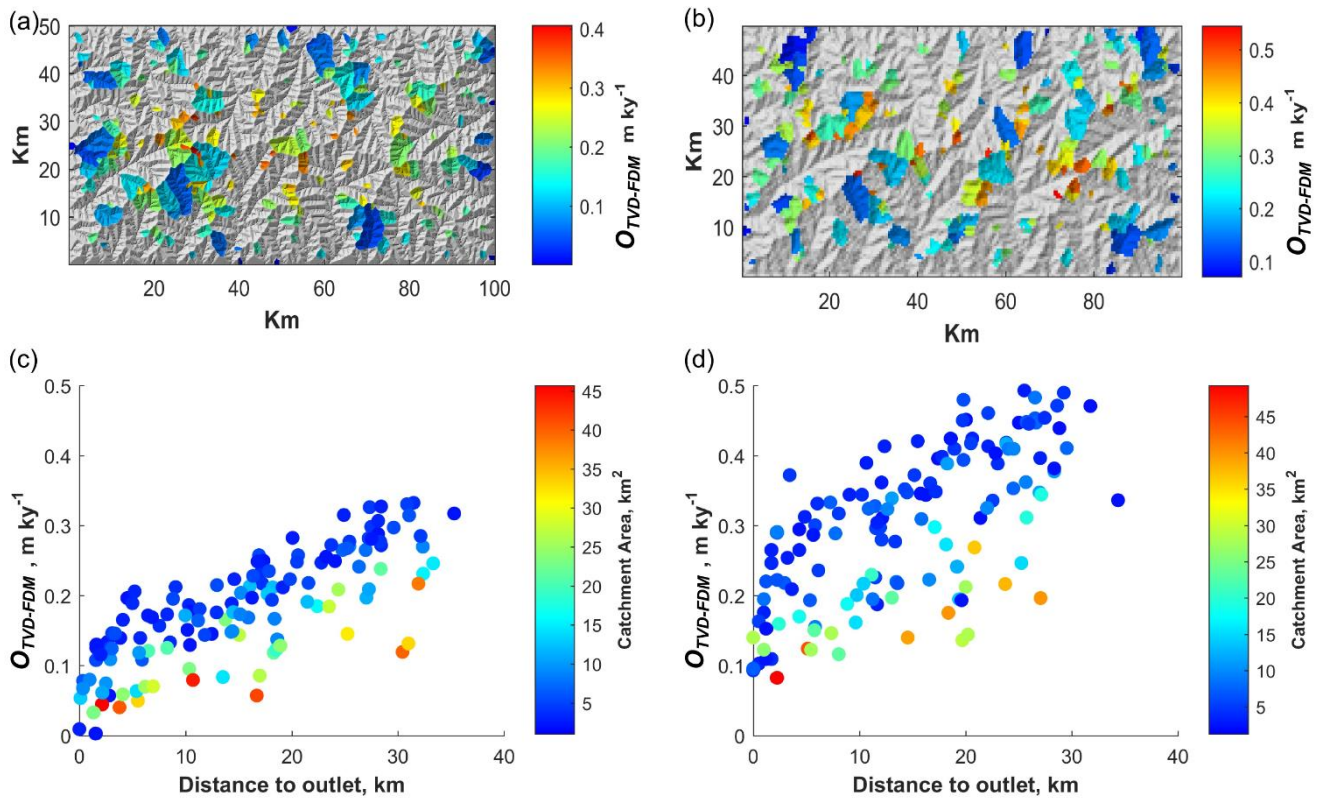
660 **Figure 7.** Spatial variation of differences between simulated erosion rates calculated with a flux limiting TVD-FVM for simulating river incision and a first order accurate implicit FDM. Here, we compare methods both run with an inner time step constrained with the CFL criterion (see text). $O_{TVD-FDM}$ is thus calculated between the black and red lines from Figure 6. Left column represents simulations run at a spatial resolution of 100 m, right column at 500 m. (a and b) Location of the randomly selected catchments with an area > 1 km² and < 50 km². Colors refer to the $O_{TVD-FDM}$ between the two simulations.

665 (c and d) Differences between the schemes increase with increasing distance from the river outlets and are inversely correlated with the catchment area.
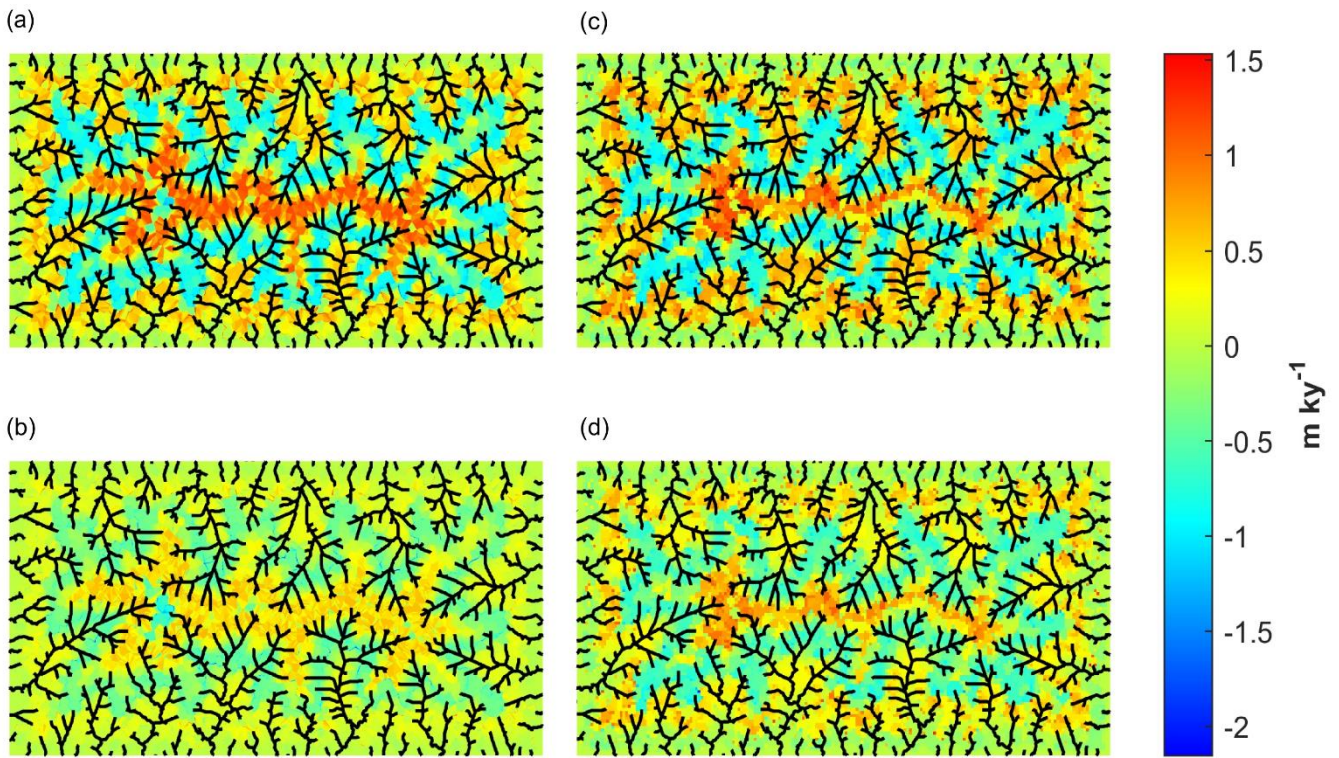
Figure 8. Spatial pattern of erosion rates during one model time step when simulating landscape evolution with the flux limiting TVD-FVM versus the first order accurate implicit FDM. (a) simulation at a resolution of 100 m where the time step of the implicit method is not constrained (b) simulation at a resolution of 100 m where the time step of the implicit method is constrained with the CFL criterion (c) simulation at a resolution of 500 m where the time step of the implicit method is not constrained (d) simulation at a resolution of 500 m where the time step of the implicit method is constrained with the CFL criterion.
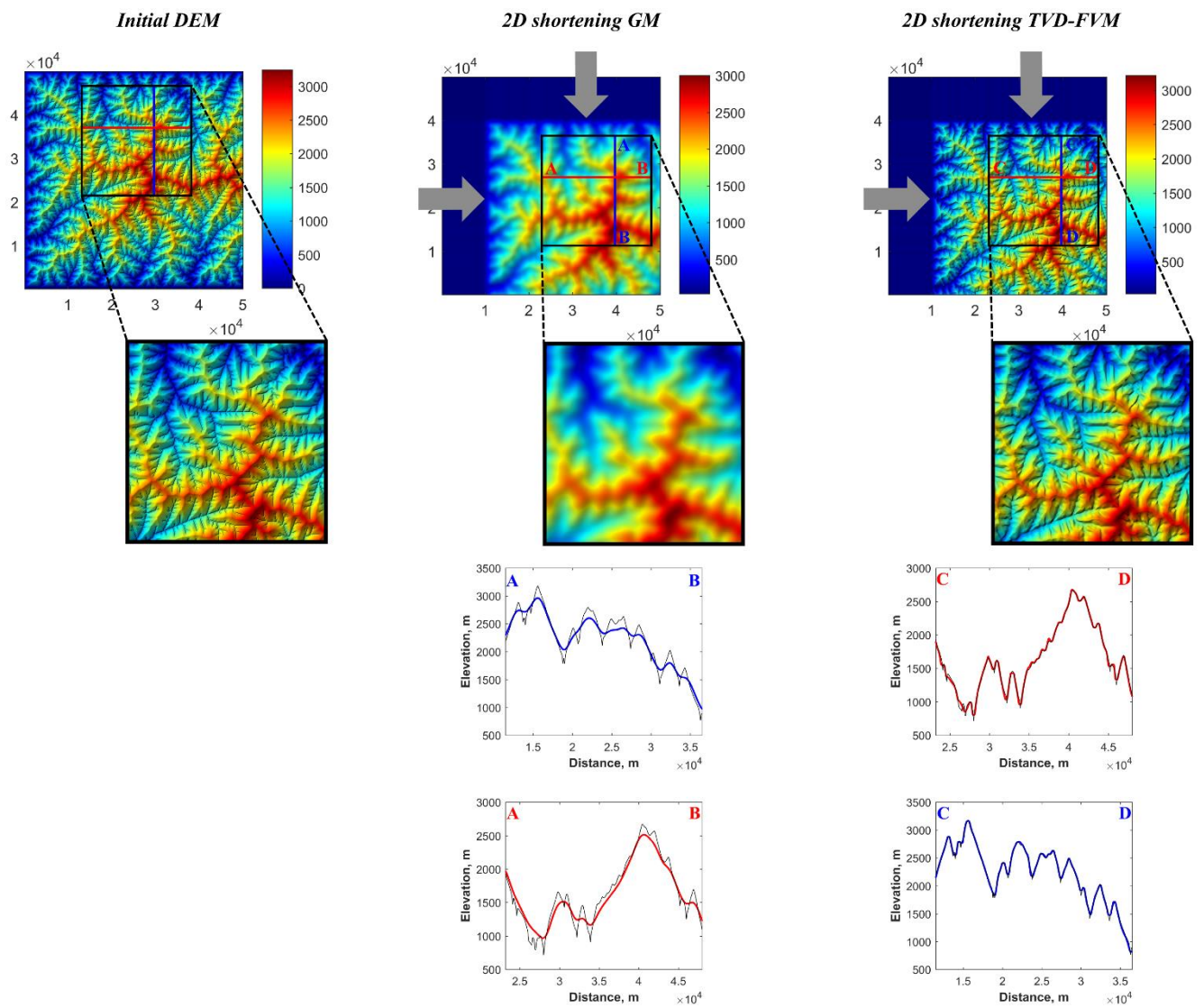
Figure 9. Impact of numerical schemes when simulating horizontal shortening on a fixed grid. Left: extract from synthetically produced DEM from Fig. 2. Middle: horizontal shortening in two directions simulated with a 2D explicit first order Godunov Method (GM). Right: horizontal shortening in two directions simulated with a 2D explicit flux limiting TVD-FVM.
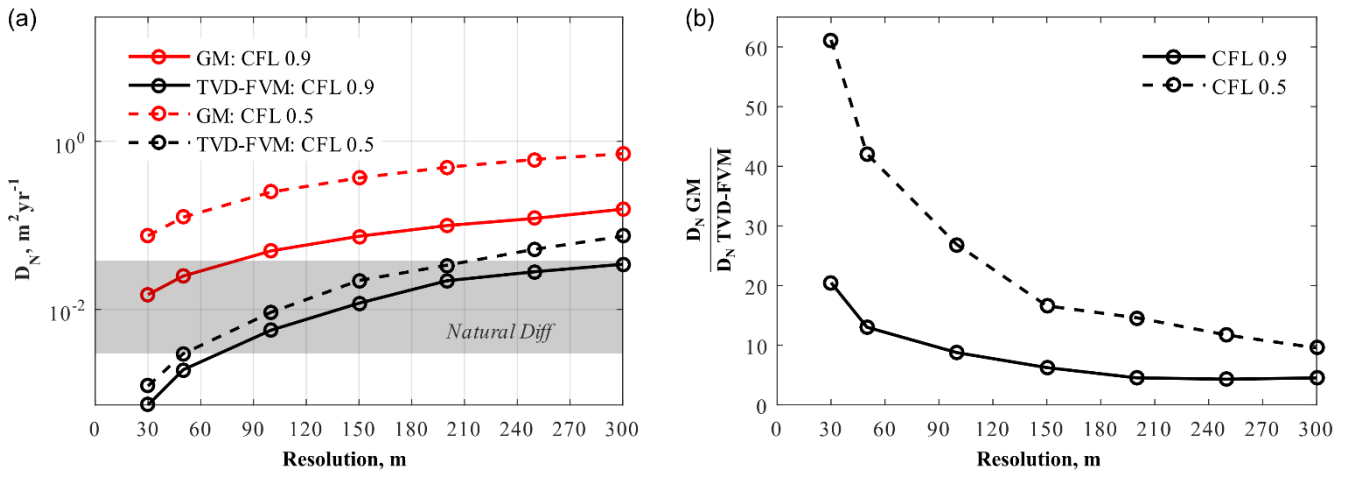
Figure 10. (a) Amount of numerical diffusion (D_N) introduced in the system when simulating lateral tectonic displacement in two directions as a function of raster resolution. The grey zone indicates the range of naturally observed diffusion rates. (b) The ratio between the amount of numerical diffusion for the first order Godunov Method (GM) versus the flux limiting TVD-FVM.

Table 1. Model parameters used for the TTLEM simulations.

Parameter	Units	Figure 1	Figure 2	Figure 4-5	Figure 6-8	Figure 9-10	Figure 2A
				Initalization			
InitialSurface		flat, 1D	random	synthetically produced DEM shown in Fig. 2	synthetically produced DEM shown in Fig. 2	synthetically produced DEM shown in Fig. 2	Big Tujunga SRTM
UpliftPattern		no uplift	uniform	uniform	uniform	Lateral Displacement	-
UpliftRate	m yr^{-1}	0	1×10^{-3}	$0 - 3\times10^{-3}$	$0 - 3\times10^{-3}$	0	0
SpatialStep	m	100	100	varying	100 - 500	varying	30
				Computational parameters			
TimeSpan	yr	1×10^6	150×10^6	1×10^6	5×10^6	1×10^6	5×10^5
TimeStep (outer)	yr	ca. 6×10^3	5×10^4	5×10^4	5×10^4	resolution dependent	1250
AreaThresh	m^2	-	5×10^4	5×10^4	5×10^4	-	5×10^4
DrainDir		-	variable	Fixed	Fixed	-	variable
SS_Value	m	-	0.5	-	-	-	-
				Boundary conditions			
BC_Type		-		Dirichlet	Dirichlet	Neumann	Neumann
BC_dir_DistSites		-		-	-	-	-
BC_dir_Dist_Value		-		1	1	-	1
BC_dir_value		-		0	0	-	0
BC_nbGhost		-		1	1	-	1
FlowBC		-		-	-	-	-
				River incision			
Kw	L^{1-2m} t^{-1}	5×10^{-6}		7×10^{-6}	7×10^{-6}	-	4×10^{-6}
m		0.42		0.42	0.42	-	0.45
n		1		1	1	-	1
				Hillslope response			
D	m^2 yr^{-1}	-		0.01	0.036	-	0.015
$\rho_r \rho_s^{-1}$	-	-		1.3	1.3	-	1.3
DiffTol		-		1×10^{-4}	1×10^{-4}	-	1×10^{-4}
Sc	m m^{-1}	-		0.8	1	-	1.2
Sc_unit		-		tangent	-	-	tangent
				Tectonic shortening			
u	m yr^{-1}			-	-	0.01	-
v	m yr^{-2}	-		-	-	0.01	-
				Numerics			
riverInc		implicit_FDM TVD_FVM		implicit_FDM	implicit_FDM TVD_FVM	-	implicit_FDM
cfls		0.9		0.9	0.9	-	0.9
diffScheme		-		Implicit linear with thresholdslope (S_c)	Implicit linear with thresholdslope (S_c)	-	Different schemes (see Fig. A2)
shortening_meth		-		-	-	Upwind_TVD Godunov Method	-

690
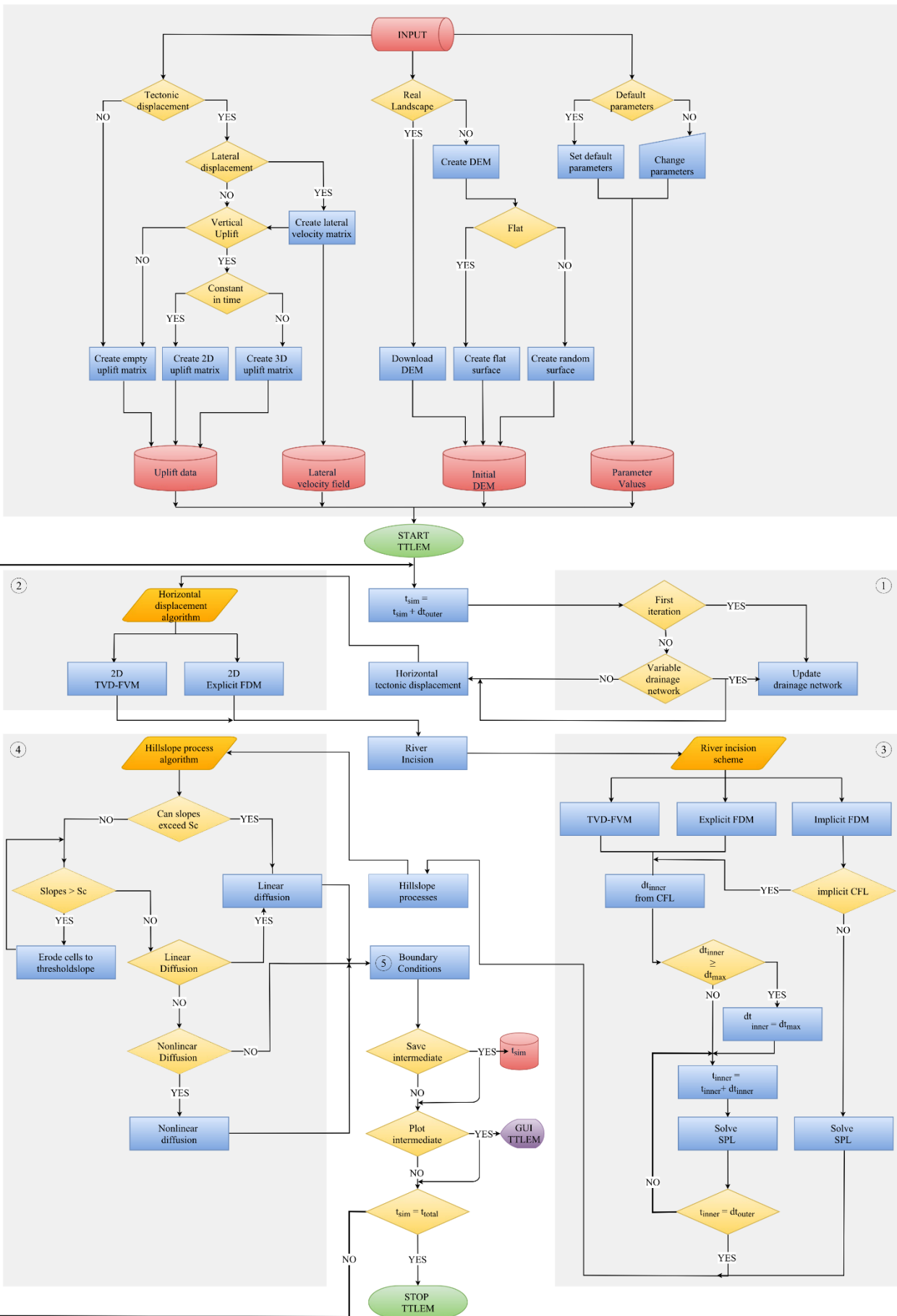
Figure A1: Schematic representation of the TTLEM model flow. The numbered methods correspond with the paragraphs from section 3 in the main text.
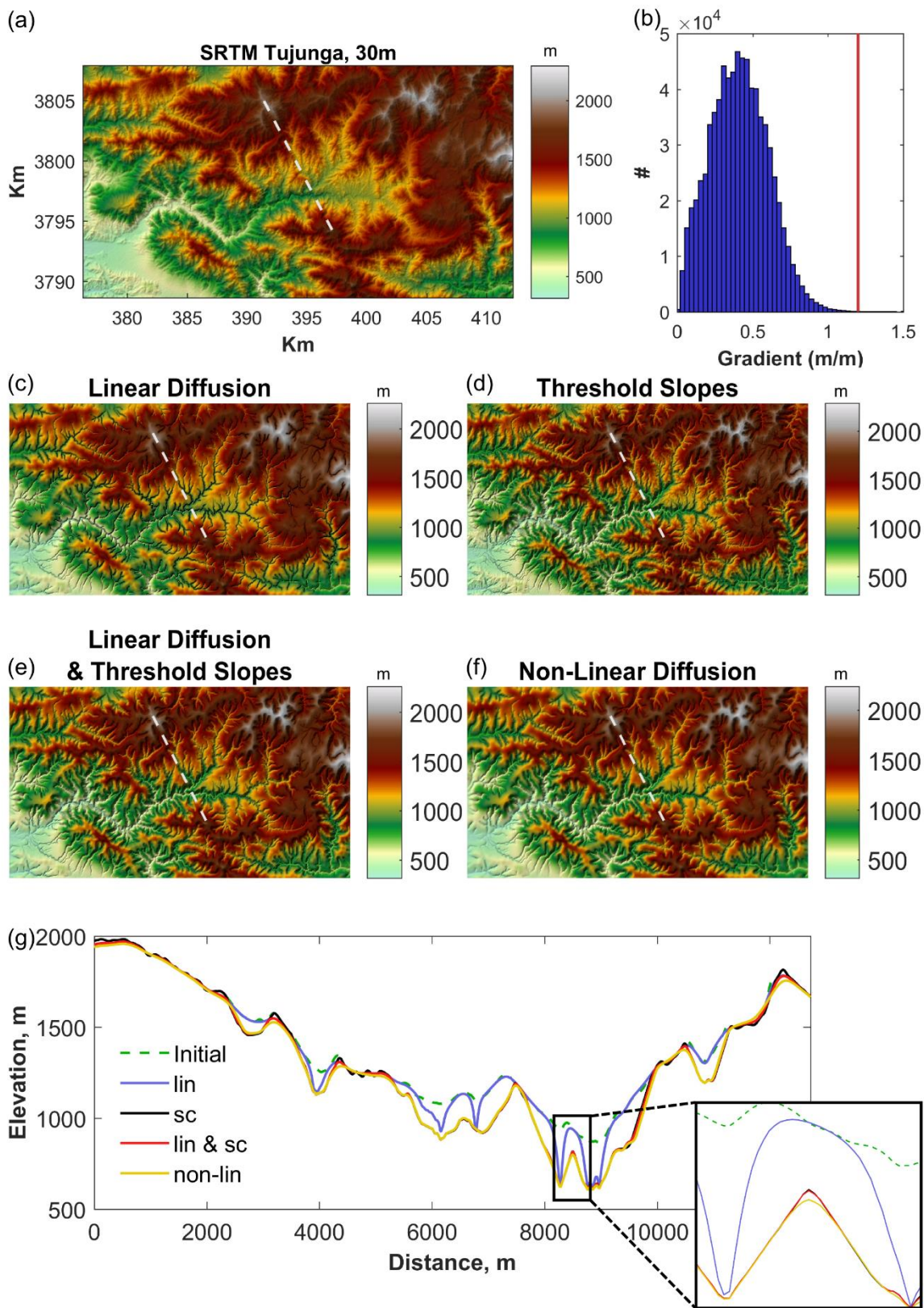
Figure A2: Hillslope response to river incision. (a) Standard SRTM DEM (30 m) included in TopoToolbox representing the Tujunga region. The dotted grey line indicates the location of the transect shown in subplot g. (b) Resulting topography after 500k years using four different descriptions for hillslope evolution. (c) Linear diffusion over all slope values (lin). (d) Threshold landscape where no slopes exceed the threshold slope (Sc). (e) Linear diffusion combined with immediate adjustment to a threshold slope (Sc). (f) Non-linear diffusion combined with immediate adjustment to a threshold slope (Sc). (g) Elevation profiles of the different model runs compared with the initial profile. Model parameter values are listed in Table 1.